Ionospheric Threats to Space-Based Augmentation System Development

S. Datta-Barua, *Stanford University*

ABSTRACT

The ionosphere contributes the largest and most unpredictable error to single frequency GPS users' range measurements. The goal of a Space-Based Augmentation System (SBAS) in mitigating these ionospheric errors is two-fold. First, the SBAS broadcasts error corrections to its users for improved positioning accuracy. Moreover, the SBAS provides a service that GPS alone cannot: ensuring position estimate integrity, which is crucial to safety-of-life applications.

The International Civil Aviation Organization (ICAO) has adopted a set of Standards and Recommended Practices (SARPs) for SBASs being developed worldwide. The SARPs are based on the Minimum Operational Performance Standards (MOPS) of the Wide Area Augmentation System (WAAS) currently operational in the United States.

This paper surveys a range of ionospheric issues that an SBAS must consider if it is to comply with the ICAO SARPs. By examining observed ionospheric phenomena at a high level in a visually intuitive way, the author hopes to provide some insight as to why the SARPs are developed as they are and what additional issues are introduced by the constraints of the SARPs.

This paper makes use of the following data: "supertruth" data collected from the WAAS network of receivers during several ionospheric storms as well as a nominal period for comparison; raw data from an individual WAAS network receiver during the 29-31 October 2003 ionospheric storm; and data from the same storm collected from nearly 400 stations in the Continuously Operating Reference Stations (CORS) and International GPS Service (IGS) networks and processed by the Jet Propulsion Laboratory (JPL).

With these data sets the author illustrates the large absolute values of total electron content (TEC), to which GPS range errors are proportional, that may be seen during ionospheric storms. Large spatial and temporal gradients that have been observed are also shown. We discuss potential routes in bounding or mitigating the effect of these highly irregular periods of ionospheric activity by considering the approach WAAS has employed.

In addition to bounding dangerous behavior that is not predicted by the SBAS choice of ionospheric model, the SBAS must also bound estimation and interpolation errors that exist both during nominal and stormy conditions. Such errors are introduced by modeling the ionosphere as a two-dimensional, infinitely thin shell. This error arises from the loss of altitudinal information in the collapse of the three spatial dimensions of the true ionosphere into a two-dimensional surface representation that can be easily broadcast.

Finally, with an ionospheric model based on measurement and estimation of the real-time ionosphere, the SBAS runs a risk of undersampling the ionosphere over a geographic region for which it is providing service, as will be illustrated. When high spatial and temporal gradients are also highly localized, it is possible for them to remain undetected by the SBAS. For this reason bounding possible errors due to undersampling is crucial.

INTRODUCTION

The ionosphere is a region of the upper atmosphere that begins at an altitude of around 50 km and extends upwards several hundred kilometers. This layer of the atmosphere is characterized by the presence of free electrons that have been stripped from atoms by solar ultraviolet radiation. As a dispersive medium, the ionosphere refracts a broadcast RF wave, say from an orbiting GPS or SBAS satellite. The delay introduced in the GPS pseudorange measurement by refraction is a function of the signal frequency and is proportional to the total electron content (TEC) along the signal path:

$$\Delta t = \frac{40.3}{cf^2}\int Ndl$$

Equation 1

The range delay error Δt is measured in seconds, c is the speed of light in vacuum, f is the signal frequency and the integral is of the number density of electrons N over the

path length of the signal [Parkinson 1996]. This error term affects GPS users' measurements worldwide and is usually on the order of meters.

Ionospheric behavior varies geographically and is generally divided into auroral, mid-latitude, and equatorial zones. These zones are roughly defined by the dominant features or processes observed in the ionosphere. The auroral regions lie near the magnetic poles beyond about 60° magnetic, equatorial regions within about 20° of the magnetic equator, and mid-latitudes in between the equatorial and auroral bands. The focus in this paper is on behavior observed in mid-latitudes. However, the topics addressed should not be considered a comprehensive list of mid-latitude ionospheric effects because during disturbed ionospheric conditions, behavior typically only seen in equatorial or auroral regions (e.g. scintillation) might actually occur in an area that is typically considered "mid-latitude". All of these types of behavior should be bounded by the SBAS, which is providing service to users over a potentially wide geographic region.

In addition to having spatial variations, the ionosphere varies temporally. "Nominal" behavior roughly follows a daily periodic pattern of higher TEC during the day, when earth is exposed to the sun's UV radiation and lower delays at night. Ionospheric behavior also varies over a longer period linked to the 11-year solar cycle. Nominal daytime peak values of TEC increase at the peak of the solar cycle. Periods of enhanced ionospheric activity and ionospheric storms are more frequent during the peak of the solar cycle. In addition to these long term temporal variations, during enhanced activity rapid rates of change in the ionospheric error term may be experienced by a GPS user. In order to maintain service integrity, the SBAS provider should be able to protect against such possibilities.

DATA AND IONOSPHERIC MEASUREMENT PROCESSING

The data used in this paper to illustrate the phenomena that an SBAS will need to bound or otherwise mitigate are of three types: 1) WAAS post-processed network data, known as "supertruth"; 2) raw dual-frequency GPS measurements obtained from one WAAS reference station receiver near Washington, D.C.; and 3) data from a network of about 400 stations distributed worldwide and collected and processed at JPL. WAAS supertruth data are used to create maps of the ionosphere to illustrate spatial gradients and two-dimensional constraints. The dual frequency receiver data is used to examine temporal gradients. The 400-station network data are used in conjunction with supertruth data to illustrate a case of an SBAS not sampling the ionosphere in a localized region of activity, thereby lacking information about it. All of the phenomena were observed over the U.S., and in all cases WAAS maintained user integrity with its currently operational correction algorithm. Specific features of this algorithm will be addressed with the topics for which they are relevant.

SUPERTRUTH DATA

The WAAS network consists of 25 reference stations, each of which has three colocated dual frequency receivers. The carrier phase ionospheric delay measurements from each of these receivers are leveled to the code in post-process. Then the data set of each receiver is checked against those of the other two receivers at the same station for agreement within tight bounds. This voting process results in "supertruth" data, a set of ionospheric delay measurements in which no biases or receiver artifacts have ever been observed.

The supertruth data contains what are known as "slant" measurements of the ionosphere because the GPS signal from a low elevation satellite spends more of its path length in the ionosphere than one that is directly overhead. To compare measurements made to satellites at various elevation angles over large geographic regions, a geometric mapping function may be used to convert slant ionospheric delays to equivalent vertical delays. In this paper a thin-shell mapping function M that treats the ionosphere as a shell is used to convert the slant delays S to equivalent vertical V:

$$M(el^k, h_{iono}) = \frac{1}{\cos(Sin^{-1}(\frac{R_e \cos(el^k)}{R_e + h_{iono}}))}$$

Equation 2

$$V = \frac{S}{M(el^k, h_{iono})}$$

Equation 3

The mapping function M is a thin shell model that is a function of the elevation of the k^{th} satellite. In the calculation of the obliquity factor M, R_e is the mean radius of the earth and h_{iono} is the assumed height of the ionospheric shell, in this case, 350 km. The point of intersection of this shell and the receiver-satellite line of sight (LOS) is known as the ionospheric pierce point (IPP). By dividing a slant delay by $M(el^k, h_{iono})$, each measurement is converted to the equivalent one a user directly under the IPP would experience if the ionosphere had no thickness and was at an altitude of 350 km.

This paper makes use of supertruth data from several days on which highly irregular ionospheric activity occurred: 6 April 2000, 15 July 2000, and 29-30 October 2003. The activity on these days is analyzed and compared with a

nominal reference day: 2 July 2000. These data are used to create maps of the ionosphere over the Conterminous United States (CONUS) to illustrate the irregular nature of ionospheric storms, spatial gradients, and constraints on modeling that exist if the SBAS broadcasts a grid of corrections and integrity bounds.

WAAS REFERENCE RECEIVER DATA

The raw dual frequency measurements from one of the WAAS reference station receivers in Washington, D.C., will be used to consider temporal gradients. TEC measurements are derived from the dual frequency data of this Novatel OEM-3 receiver. The carrier phase measurement of total electron content between the receiver and one satellite, expressed in meters of slant delay at L1, is $S_{L1,\phi}$:

$$S_{L1,\phi} = \frac{f_{L2}^2}{f_{L1}^2 - f_{L2}^2}[\lambda_{L1}(\phi_{L1} - N_{L1}) - \lambda_{L2}(\phi_{L2} - N_{L2})]$$

Equation 4

The carrier phase measurements to the satellite, in number of cycles at the L1 and L2 frequencies are φ_{L1} and φ_{L2}, respectively. The frequencies of the L1 and L2 bands are denoted f_{L1} and f_{L2}, and the wavelengths are λ_{L1} and λ_{L2}, in meters. The carrier phase measurement $S_{L1,\varphi}$ provides a low-noise measure of the slant ionospheric delay, but is ambiguous due to the unknown integer number of wavelengths N_{L1} and N_{L2} of the carrier phase at each frequency. For this reason it is leveled to the coarser but unambiguous code measurement of the ionospheric delay, $S_{L1,\rho}$:

$$S_{L1,\rho} = \frac{f_{L2}^2}{f_{L1}^2 - f_{L2}^2}(\rho_{L2} - \rho_{L1})$$

Equation 5

In these equations, ρ_{L1} and ρ_{L2} are the receiver pseudorange measurements, in meters, to the satellite at the L1 and L2 frequencies, respectively. The ionosphere is dispersive, and higher frequencies (i.e. carrier signals φ_{L1} and φ_{L2}) are advanced by an amount equal and opposite to the delay at lower frequencies (i.e. chipping rates of code ρ_{L1} and ρ_{L2}), so the signs for $S_{L1,\rho}$ and $S_{L1,\phi}$ are opposite. By taking advantage of the carrier advance and code delay, a single frequency measurement of the ionospheric delay, $S_{L1,ccd}$, can be made:

$$S_{L1,ccd} = \frac{\rho_{L1} - \lambda_{L1}(\phi_{L1} - N_{L1})}{2}$$

Equation 6

Again, the carrier phase measurement φ_{L1} is ambiguous due to the unknown integer number of cycles N_{L1}, so $S_{L1,ccd}$ is also leveled to the code measurement of delay, $S_{L1,\rho}$. Examining code-carrier divergence at the L1 frequency is a way of avoiding carrier phase cycle slips, which are much rarer on L1 than L2. The WAAS receiver data examined in this paper was collected on 30 October 2003 during one of the strongest storm periods observed. In the WAAS reference receiver data used in this paper, no cycle slips were observed, so no algorithm for repair was required.

CORS NETWORK DATA

The U.S. National Geodetic Survey makes data publicly available from a network of Continuously Operating Reference Stations (CORS). The data collected from these stations during the 29-31 October 2003 storm have been assimilated and leveled by the use of the Global Ionospheric Mapping (GIM) software at NASA's Jet Propulsion Laboratory (JPL). With the additional use of publicly available International GPS Service (IGS) station data worldwide, GIM estimates and removes satellite and receiver interfrequency biases to provide high precision ionosphere measurements. The processing is described in detail by Komjathy et al [2002 and 2003].

IONOSPHERIC STORMS

An example of nominal ionospheric behavior, as described in the introduction, is illustrated in Figure 1. A map of nominal ionospheric behavior on 2 July 2000 at 21:40 UT, over the U.S. was obtained from WAAS supertruth data. The axes indicate latitude and longitude in degrees, with positive north and east. Each circle marks an IPP and has a line segment pointing to the reference station with which it is associated. The length of the line segment is inversely proportional to the elevation of the satellite. The IPP is assigned a color according to its equivalent vertical ionospheric delay from 0 m (blue) to 10 m (red). The map color contours are interpolated by determining a plane within each set of three nearest IPPs.

This map of typical behavior demonstrates that, on the whole, the nominal ionosphere varies smoothly over a large region. This allows the SBAS to model and estimate the nominal ionosphere with reasonable confidence.

The challenge is to determine in real-time whether the ionosphere is instead behaving as shown in Figure 2, and protect users from delays of the magnitudes and variations shown there. Figure 2 is a snapshot of the ionosphere taken from WAAS supertruth data on 29 October 2003, at 21:40 UT, during the height of an ionospheric storm. The color scale in this figure differs from the previous figure: red now corresponds to an equivalent vertical ionospheric delay of *35 m*.

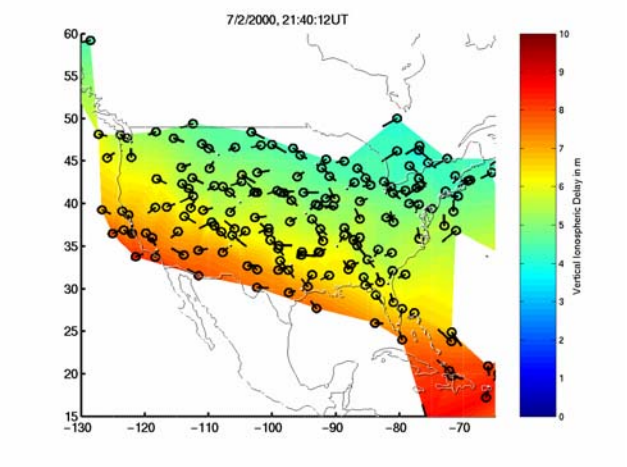

Figure 1: Contour map of nominal ionosphere over the United States. Colors range from 0 to 10 m of equivalent vertical range delay.

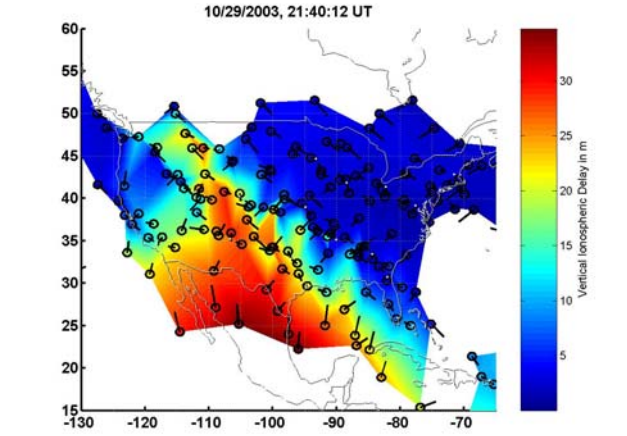

Figure 2: Contour map of severely disturbed ionosphere observed over the United States. Colors range from 0 to 35 m of equivalent vertical range delay.

In Figure 2 the ionosphere does not vary in a smooth planar manner over hundreds of kilometers. Also, the absolute values of ionospheric delay are among the highest observed, approaching the nearly 45 m measured later during this same storm as well as the 15 July 2000 storm. The IPPs with equivalent vertical delays of 35 m at the south of the map are associated with fairly low elevation satellites, so the signal path delay experienced by the receiver may actually be a factor of 2 or 3 more.

For an SBAS to provide integrity to its users, the system must either model behavior such as that shown in Figure 2 accurately and be able to broadcast that information to its users in real-time with bounds that will cover the spatial variability observed or, if the SBAS ionospheric threat model fails to accurately represent disturbed behavior, it must have a detection system of some kind in place to warn that the model cannot be safely used. This is the motivation behind the WAAS irregularity detector, which provides a robust warning system when the ionospheric model cannot safely be used with the observations made, during which time the broadcast message from WAAS is "Do Not Use" [Walter 2000].

SPATIAL GRADIENTS

The SBAS offers service over a large geographic region. Users may be hundreds of kilometers from the nearest SBAS reference station. The ionospheric delay they suffer could be very different from that which the reference station measures depending on their proximity to the reference station. To provide confidence levels on broadcast ionospheric corrections, a measure of how different a nearby user's delay could be, i.e. a spatial decorrelation rate, must be included.

During disturbed periods, the user near to the reference station may experience a very different delay without being very far away. Without a way to distinguish that a region is under a disturbed ionosphere (i.e. an irregularity detector), the SBAS must bound the highest possible spatial decorrelation rates for all users at all times if it is to ensure integrity.

Figure 3 shows a contour map that delineates the location at which a high spatial decorrelation rate was observed. The supertruth data plotted are over the mid-Atlantic coastal U.S. during an ionospheric storm period on 6 April 2000. Latitude and longitude are marked on the axes, with degrees north and east positive. The WAAS reference stations (WRS's) in this region are marked with a star (*). The only IPPs plotted explicitly are the ones associated with svn 40, and the small magenta lines in the IPP circles point toward the associated WRS.

This contour map differs from the previous figures because it is not simply a snapshot of the IPP measurements at a single epoch. Instead, the IPP measurements at both UT 21:32:12 and 21:34:02 contribute to a composite contour map interpolated by a standard plotting routine between the IPPs. The goal is to show that along the LOS between the WRS at Washington, D.C., and svn 40, a change in vertical ionospheric delay of 6 m was recorded as the IPP position shifted 7 km. The plot illustrates a very clear curve separating the light green (10 m) and dark blue (4 m) regions as the IPP at 38° N, 79° W, crossed an ionospheric spatial irregularity.

Previous analysis of the supertruth data showed that, by accounting for the approximate speed of the ionospheric storm front, the decorrelation could be revised to 6 m over 19 km [Datta-Barua]. Although subsequent analysis of

this event refined estimates of the spatial gradient observed here to be 6 m/75 km, or 80 mm/km [Luo et al 2003], further research into other storms has demonstrated the existence of spatial gradients of 200, 300, and even 400 mm/km [Luo 2004, Dehel 2004]. WAAS successfully contended with these features through the use of its storm detector, which notified users in this region not to use WAAS until the storm conditions had subsided.

Without the irregularity detector, WAAS would need to broadcast overbounds on the few hundred mm/km spatial decorrelation rate for all its users all the time. This would hurt overall availability. Without a storm detector that robustly declares periods of disturbed activity, the general SBAS would need to assume these conditions could happen to any user at any time anywhere within the region of coverage.

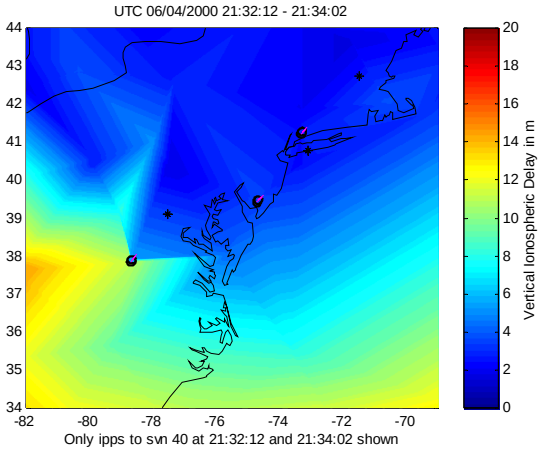

Figure 3: Time-lapse map of east Atlantic CONUS. The IPP at 38° N, 79° W crosses the ionospheric storm front.

TEMPORAL GRADIENTS

An SBAS whose ionospheric model is based on real-time data broadcasts a correction update periodically at discrete time intervals. Time-dependent changes in the ionosphere may degrade or even obsolesce the old broadcast message before a new one is available to the user. For that reason a bound on temporal gradients must be included in the integrity bounds to protect users from potentially hazardous rates of change that may occur at the users' lines of sight. These bounds must cover all possible temporal gradients when the SBAS offers service.

The supertruth data for 2 July 2000 provides an example of the magnitude of temporal decorrelation rates during nominal conditions. A histogram of the rates of change of ionosphere observed by WAAS on this day is shown in Figure 4, with the probability of occurrence plotted on a logarithmic scale. On 2 July 2000 the most extreme rates of change observed were under 8 mm/s. To provide service during nominal periods, an SBAS would need to provide integrity bounds on this behavior, as WAAS does.

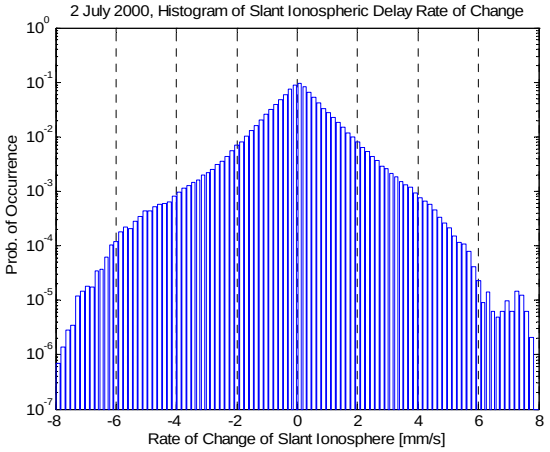

Figure 4: Nominal ionospheric decorrelation rates in mm/s observed by WAAS on 2 July 2000.

SBAS users also need to be protected from the possibility of an event such as the one shown in Figure 5. Figure 5(a) is a plot of slant ionospheric delay in meters as a function of time in seconds, measured from a WAAS reference receiver at Washington, D.C., as an ionospheric feature caused the range delay to change rapidly. The dotted black line is the code measurement of the delay, $S_{L1,\rho}$ (Equation 5), the dashed red curve is the carrier measurement $S_{L1,\varphi}$ (Equation 4), and the solid blue curve is one-half the code-carrier divergence, $S_{L1,ccd}$ (Equation 6). Figure 5(b) is a plot of the rate of change of the slant delay $S_{L1,ccd}$, computed by taking the difference between each epoch and the epoch 100 seconds later to reduce the effects of noise.

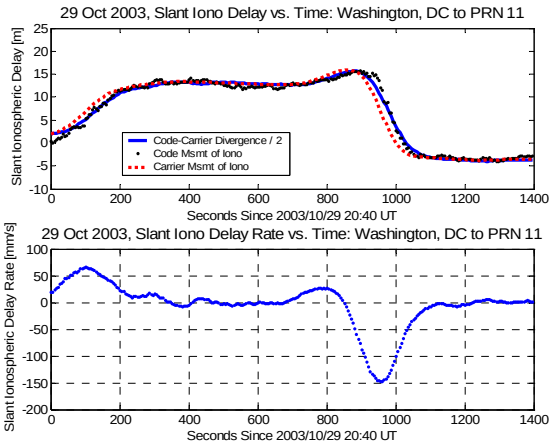

Figure 5: Severe temporal gradients observed by WAAS reference receiver. (a) Slant ionospheric delay [m] vs. time [s]. (b) Rate of change of slant ionospheric delay [mm/s].

Notice that during this period, the receiver experienced a rate of change in range delay error as high as 150 mm/s. However, this rate of change is a mixture of the purely temporal variation of the ionosphere and the apparent variation due the motion of the LOS through a spatial gradient. A similar analysis to the ones done to consider spatial gradients might show that by accounting for the relative motion of the IPPs and the ionospheric feature, the rate would actually be lower.

However, this rate of change would need to be bounded for all users of the SBAS, regardless of the motion of their IPPs. Therefore, the user whose LOS has the worst possible relative motion with respect to the ionospheric spatial feature, similar to that shown here, could expect to see a temporal gradient of this order of magnitude. The SBAS must consider whether it will incorporate the worst possible relative motion of the LOS into the calculation of integrity bounds or leave the onus of accounting for the relative motion to each individual user.

Without some way of determining in real-time that a region is disturbed (such as an irregularity detector), the SBAS would need to treat high temporal gradients as a possibility for all users at all times, and thus, broadcast integrity bounds high enough to cover this rate of change. As with the spatial gradients and non-planar irregular behavior addressed above, WAAS protected users from these extreme events with the use of a storm detector, and provided integrity correction bounds during nominal periods that did not trip the storm detector, such as 2 July 2000.

THIN SHELL LIMITATIONS

The ICAO SARPs specify that a grid of ionospheric error corrections and bounds be broadcast. In order to represent the ionosphere as a grid, the SARPs specify that the thin-shell model described in the introduction, with the obliquity factor given by Equation 2 where the shell height h_{iono} = 350 km, must be used.

This representation of the ionosphere has limitations that remain even during the quietest, most nominal ionospheric behavior. One particular issue is that, by collapsing the three-dimensional ionosphere of several hundred kilometers' thickness into a two-dimensional shell, vertical information is lost. In other words, if two lines of sight from different receivers in the network intersect each other at an altitude of 350 km, they have the exact same IPP location. Conceptually, the lines of sight form an "X," and the signals travel through very different regions of the ionosphere. As a result they may have very different range delay values, even though the IPPs appear at the same point on a map. This is a limitation inherent to the thin shell model. The difference between two IPPs on the shell may not vanish in the limit when they are colocated because their "look angles" may be completely different.

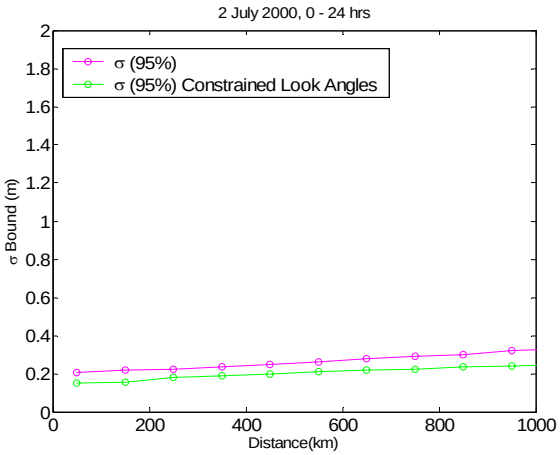

Figure 6: Normalized 95th percentile standard deviation of equivalent vertical range delay differences (m) vs. IPP separation distance (km) on a nominal day. Magenta: all possible pairs of IPPs. Green: IPPs with $\Delta el \leq 15°$ and $\Delta az \leq 15°$.

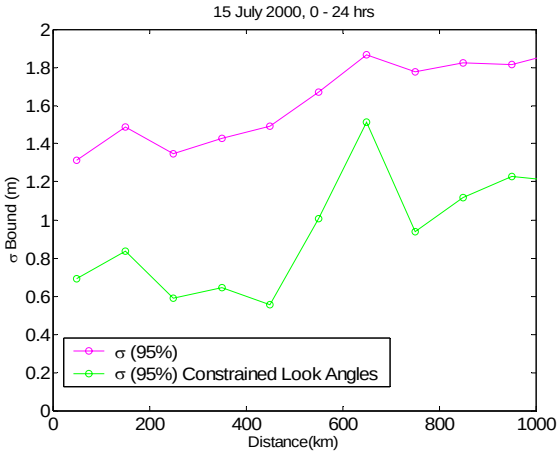

Figure 7: 95th percentile standard deviation of equivalent vertical range delay differences (m) vs. IPP separation distance (km) on a disturbed day. Magenta: all possible pairs of IPPs. Green: IPPs with $\Delta el \leq 15°$ and $\Delta az \leq 15°$.

Figure 6 and Figure 7 serve to illustrate this point for a nominal day and stormy day, respectively, as obtained from the WAAS supertruth data. The analysis and production of these plots was performed by Rajagopal, and is described in detail in his earlier work on the subject [2003]. Briefly, at each epoch every possible pair of IPPs is placed into a bin in a two-dimensional histogram based on 1) the difference in vertical delay and 2) the separation distance between them. At each distance bin (spanning 100 km each), the 95th percentile (2-sigma) bound on the difference in vertical delay between IPPs is found and

normalized to a 1-sigma value by dividing by two. These bounds are plotted in magenta as a function of IPP separation distance. The green curve places additional requirements on the IPP pair: the elevation angles must lie within 15° of each other, as must the azimuthal angles. This enforces that they have similar look angles before they are counted in the histogram. The 95th percentile of these points are obtained and plotted in green.

There are a number of interesting conclusions illustrated in these two plots. For the nominal day of 2 July 2000, Figure 6 shows that the sigma bound, when counting all possible pairs (magenta), does not in fact approach the origin. Instead on this quiet ionosphere day, as the IPPs become closer together, the difference between them may vary by a fraction of a meter. If the only IPP pairs counted are the ones whose elevation angles and the azimuth angles lie within 15° of each other, then the sigma bound is somewhat reduced.

The same general trend is true on the stormy day 15 July 2000, illustrated in Figure 7. Counting all possible pairs of IPPs results in a sigma bound on the vertical delay difference of about 1.2 m at 0 km separation. Limiting the analysis to pairs with similar look angles reduces this difference bound to roughly 0.7 m at 0 km separation. The irregular behavior of the ionosphere on the storm day contributes to the inflation of the bounds seen in Figure 7 as compared to the quiet day shown in Figure 6.

UNDERSAMPLING

Since the SBAS uses a data-driven model of the ionosphere, it will have to contend with the threat of undersampling. The SBAS developers will need to factor in the probability that there is some feature in the ionosphere that is not detected by the reference receivers. This feature may lie just beyond the view of the receiver network, or it may be an even more insidious threat, one that just happens to fit right in between the measurements of the reference stations. In the latter case the ionosphere may seem to be well-sampled when in fact it is not. A comparison of the next two figures illustrates this point dramatically.

Figure 8 shows a contour map, generated in the same way as Figures 1 and 2, of the IPPs recorded by supertruth on 30 October 2003 at 05:50 UT. The contour colors are interpolated with standard plotting routines that determine a plane for each set of three nearest pierce points. These contour colors serve merely to give an idea of what information WAAS had available to it in real-time, and what that looks like when viewed in this simple manner. The IPPs are denoted with black circles, and their associated receivers lie in the direction of the line segments. Longer line segments indicate that the satellite is at a low elevation. The color scale varies from 0 to 20 m.

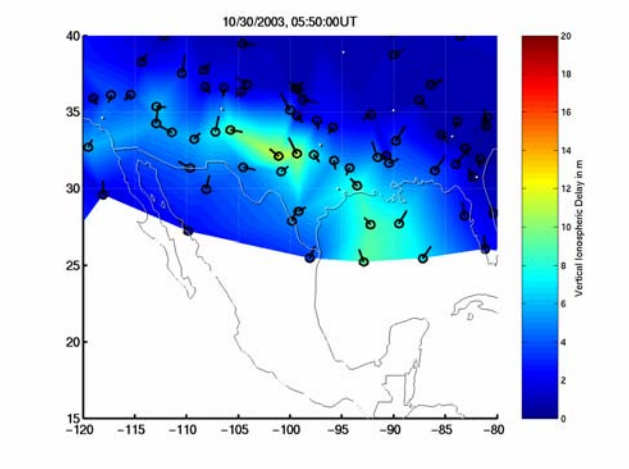

Figure 8: Contour map of the ionosphere over the southern U.S. generated by standard plotting routines based on supertruth data recorded 30 October 2003.

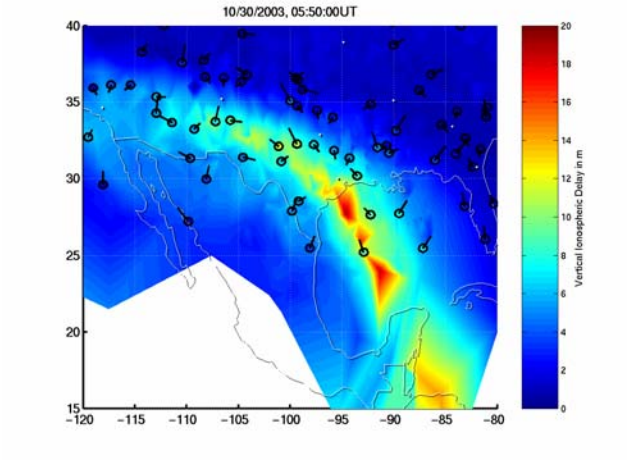

Figure 9: Contour map of the ionosphere based on CORS network data. Plotted on top of this are circles denoting the IPPs recorded by WAAS (same set as in Figure 8).

On the whole the map is relatively quiet, since it is a snapshot of local night-time, although even an equivalent vertical delay value of 5 m (blue) is higher than usual at mid-latitude local nighttime. There are indications of irregular behavior over Texas and at the edge of the sampled region, over the Gulf of Mexico.

Now for comparison, at the same epoch a contour map based on the high-density CORS network data is shown in Figure 9. Overplotted on this CORS contour map are the very same WAAS IPPs shown in Figure 8. The CORS measurements indicate that there is a localized region of the ionosphere where equivalent vertical delays of 20 m were measured. This map shows that the WAAS IPPs at

this epoch hovered just on the edges of this irregularity. In one case, the IPP at 25° N, 93° W, sampled in the same thin shell location as this irregularity. However, the delay measured at that point was less than in surrounding areas. For this IPP, the WAAS reference station viewed a low elevation satellite (indicated by the longer line segment). It appears that this LOS passed right *under* the irregularity.

Another point worth mentioning is that what may have appeared to be two different features colored green in Figure 8 was more likely a continuation of one larger structure. The apparent distinctness of the two green areas in Figure 8 is an artifact of the contour plotting method. It is worth bearing in mind that this simplistic type of contour is not what the WAAS ionospheric correction algorithms are based on. This contour plot says nothing about the confidence with which colors are assigned. That is the fundamental advantage to the SBAS estimates. An SBAS offers more than just a best guess of the ionospheric error based on whatever measurements are available. In addition it offers a guarantee on the worst that the true ionosphere can be for a user, based on the measurements. In the case shown in Figures 8 and 9, the bounds would need to cover the unobserved 20 m vertical delay.

An additional challenge of contending with undersampling threats is that, in order for the SBAS to meet FAA certification requirements, its overall broadcast integrity bound must be sufficient for any combination of IPPs. Since the SBAS has users over a wide geographic region and has no knowledge of where the users' IPPs are, it must protect them from possible ionospheric features, no matter what distribution of ionospheric pierce points it measures.

SBAS developers can address this issue of protecting users given any possible sampling of the ionosphere through the use of data deprivation. The goal of data deprivation is to simulate scenarios in which the SBAS would have sampled the ionosphere insufficiently in a threatening area (as it did in Figure 8 and Figure 9) and assess the resulting severity of the threat to the user. SBAS designers must then develop an undersampling bound that protects up to the most severe of these threats.

Figure 10 and Figure 11 illustrate a scenario artificially created by deprivation that mimics the physical situation that was observed in Figure 8 and Figure 9. In Figure 10 a contour map of equivalent vertical delay (0-10 m) is plotted with standard visualization routines using all CORS data available at 05:00 UT on October 31, 2003. The feature over Florida was sampled by WAAS as well, but for plotting purposes CORS data is more complete. One particular choice of data deprivation schemes (many are possible) is applied to the WAAS supertruth data at this epoch, and the IPPs that are not excluded by this process are plotted with circles and lines directed toward the receiver making the measurement. The excluded supertruth IPP data, though not indicated with circles, are all located in the red-yellow region over Florida in the contour map.

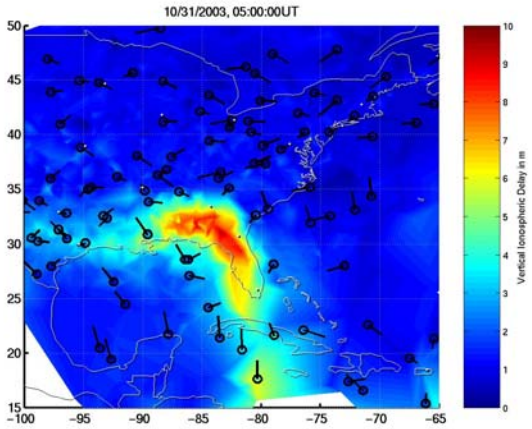

Figure 10: Contour map of the ionosphere over the eastern US based on CORS data. Plotted over the contours are supertruth IPPs that were *not* excluded by data deprivation.

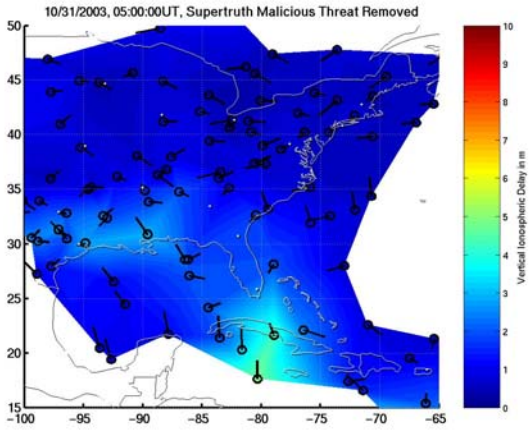

Figure 11: Contour map of the ionosphere over the eastern US based on supertruth data not excluded by data deprivation. IPPs that were not excluded (same set as in Figure 10) are marked with circles.

In contrast, Figure 11 shows what the contour map would look like based on the WAAS measurements without these excluded IPPs. As a result of this combination of IPPs, not only does activity appear to be generally calm over Florida, but the region appears to be relatively well-sampled: the gap in measurements over Florida is not much larger than the undeprived hole over the Gulf of Mexico. There are measurements of about 2.5-3.5 m on all sides, which would all seem to confirm that nothing

unusual is occurring over Florida. For this distribution of IPPs, even though the region seems well-sampled, the ionosphere varies quite a bit, and the SBAS would need to protect users from this possibility.

Ideally, the SBAS developers would do an exhaustive search over all possible combinations of IPPs, but this is prohibitively time-consuming and computationally expensive. One possible and extremely conservative deprivation technique is to search for precisely those combinations of IPPs that would give the most trouble to the SBAS model – create a scenario that fools the system in the worst possible way, and make sure that that scenario is protected by the undersampling bound.

CONCLUSIONS

A successful SBAS bounds the threats illustrated in this paper to maintain user integrity while keeping availability high. The threats to integrity with which the SBAS must contend include highly nonplanar and localized irregular behavior, as is seen during the 29-31 October 2003 storm. This period introduced equivalent vertical delays of as much as 45 m in some areas of CONUS; user slant delays would have been as much as a factor of 2 to 3 higher. Behavior which indicates a breakdown of the ionospheric model (in the WAAS case, the planar fit) should be mitigated by the use of some form of irregularity, or "storm," detector.

At all times while providing service, confidence bounds must be broadcast on spatial gradients since users are not colocated with reference stations. During disturbed conditions, spatial gradients as high as 400 mm/km have been observed. The SBAS must also place bounds on temporal gradients since the broadcast message has a usable life on the order of a few minutes. In this paper temporal gradients on the order of 150 mm/s are illustrated. Future work may include revising the temporal gradient to a lower value by accounting for the user and IPP geometry, as has been done by others with regard to the spatial gradient. However, the problem of gradients being coupled to user geometry remains one that must be protected against. The SBAS must decide whether bounding the worst possible geometry in conjunction with these gradients is within the scope of its functionality or whether the burden of the geometric calculation must ultimately be assigned to the user.

Modeling limitations imposed by the ICAO SARPs broadcast message specification must all be taken into account when the SBAS provides integrity. In particular, one outcome of using the thin-shell model is that even colocated IPPs may have entirely different equivalent vertical delays. More than a spatial gradient, this can be interpreted as a look-angle decorrelation. The SBAS must protect users from using an estimate of the ionosphere based on measurements taken from very different elevation and azimuth angles than theirs.

Finally, the threat of undersampling the ionosphere was illustrated for any data-driven model. A specific instance of an SBAS barely detecting a significant feature was pointed out. It is precisely for such cases that the WAAS ionospheric threat algorithm includes a sigma bound on undersampling. Data deprivation simulates undersampling scenarios to allow for threat assessment and development of bounds. Each of the threats mentioned in this paper have been bounded or mitigated by WAAS, and any future SBAS offering integrity will need to address all of these issues as well. Once the crucial service of integrity has been provided to users, the next step will be to continue to maintain it while increasing availability.

ACKNOWLEDGEMENTS

The author would like to thank the FAA WAAS program for funding this research. Thanks also to the following people: Attila Komjathy at JPL for providing the processed data from the 400 CORS and IGS stations and the recovered WAAS supertruth data; Karl Shallberg at Zeta Associates, Inc., for providing the dual-frequency data; Sriram Rajagopal for providing the plots of decorrelation rates; and Todd Walter for providing helpful feedback and comments.

REFERENCES

Christie, J.R.I., P. Ko, B. Pervan, P. Enge, J.D. Powell, and B. Parkinson, "Analytical and Experimental Observations of Ionospheric and Tropospheric Decorrelation Effects for Differential Satellite Navigation during Precision Approach," Proceedings of ION GPS 1998, p. 739-748.

Datta-Barua, S., T. Walter, S. Pullen, et al., "Using WAAS Ionospheric Measurements to Estimate LAAS Short Baseline Gradients," Proceedings of ION NTM 2002, San Diego, California, 28-30 January 2002, p. 523-530.

Dehel, T., F. Lorge, J. Warburton, "Satellite Navigation vs. the Ionosphere: Where Are We, and Where Are We Going?" Proceedings of ION GNSS 2004, Long Beach, California, 21-24 September 2004.

Foster, J. C., "Quantitative Investigation of Ionospheric Density Gradients at Mid Latitudes," Proceedings of ION NTM 2000, Anaheim, California, 26-28 January 2000, p. 447-453.

Hansen, A., Peterson, E., Walter, T., and Enge, P., "Correlation Structure of Ionospheric Estimation and

Correlation for WAAS", in Proceedings of ION NTM, Anaheim, CA, January 2000.

Klobuchar, J. A., P.H. Doherty, and M. B. El-Arini, "Potential Ionospheric Limitations to Wide-Area Differential GPS," Proceedings of ION GPS 1993, Salt Lake City, Utah, p. 1245-1254.

Komjathy, A., L. Sparks, A.J. Mannucci, and X. Pi, "An Assessment of the Current WAAS Ionospheric Correction Algorithm in the South American Region," Proceedings of ION GPS 2002, Portland, Oregon, 24-27 September 2002, p. 1286-1296.

Komjathy, A., L. Sparks, A. J. Mannucci, and X. Pi, "On the Ionospheric Impact of Recent Storm Events on Satellite-Based Augmentation Systems in Middle and Low-Latitude Sectors," Proceedings of ION GPS/GNSS 2003, Portland, Oregon, 9-12 September 2003, p. 2769-2776.

Luo, M., S. Pullen, J. Dennis, et al., "LAAS Ionosphere Spatial Gradient Threat Model and Impact of LGF and Airborne Monitoring," ION GPS/GNSS 2003, Portland, Oregon, 9-12 September 2003, p. 2255-2274.

Luo, M., S. Pullen, A. Ene, et al., "Ionosphere Threat to LAAS: Updated Threat Model and Future Solutions," Proceedings of ION GNSS 2004, Long Beach, California, 21-24 September 2004.

Misra, P., and Enge, P., *Global Positioning System: Signals, Measurement, Performance*, Ganga-Jamuna Press: Lincoln, Massachusetts, 2001.

Parkinson, B.W., J. J. Spilker, P. Axelrad, and P. Enge eds., *Global Positioning System: Theory and Applications*, vol. 1-2, American Institute of Aeronautics andAstronautics, Washington, D.C., 1996, p. 485-515.

Rajagopal, S., T. Walter, S. Datta-Barua, J. Blanch, T. Sakai, "Correlation Structure of the Equatorial Ionosphere," Proceedings of ION NTM 2004, San Diego, California.

Sparks, L., X. Pi, A.J. Mannucci, et al., "The WAAS Ionospheric Threat Model," Proceedings of the International Beacon Satellite Symposium, Chestnut Hill, Massachusetts, 4-6 June 2001, p. 237-241.

WAAS MOPS (1999). "Minimum Operational Performance Standards for Global Positioning System / Wide Area Augmentation System Airborne Equipment." RTCA Inc. Document No. RTCA/DO-229B, October 6.

Walter, T., A. Hansen, J. Blanch, et al., "Robust Detection of Ionospheric Irregularities," ION GPS 2000, Salt Lake City, Utah, 19-22 September 2000, p. 209-218.